AGU ADVANCING EARTH AND SPACE SCIENCES

Geophysical Research Letters

RESEARCH LETTER
10.1029/2025GL119921

Spatial Patterns of Shallow Clouds: Challenging the Concept of Defined Regimes

Giovanni Biagioli[1,2], Giulio Mandorli[3], Lilli Johanna Freischem[4], Alejandro Casallas[1,5], and Adrian Mark Tompkins[1]

[1]Earth System Physics, International Centre for Theoretical Physics (ICTP), Trieste, Italy, [2]Now at Laboratoire de Météorologie Dynamique/Institut Pierre-Simon Laplace (LMD/IPSL), Sorbonne Université, CNRS, Paris, France, [3]Laboratoire de Météorologie Dynamique/Institut Pierre-Simon Laplace (LMD/IPSL), Sorbonne Université, CNRS, Paris, France, [4]Atmospheric, Oceanic and Planetary Physics, University of Oxford, Oxford, UK, [5]Institute of Science and Technology Austria, Klosterneuburg, Austria

Abstract Tropical shallow clouds are a major source of uncertainty in Earth's climate sensitivity, especially through their spatial arrangement, which global climate models do not represent. Efforts to understand their organization have partly relied on classifying observed scenes, identifying four patterns as archetypal regimes. Here we analyze geostationary satellite imagery of the western tropical Atlantic using the *L*-function, a tool based on point pattern theory that quantifies cloud organization across spatial scales. Classical examples of the four patterns show distinct *L*-function fingerprints, revealing their characteristic clustering and regularity scales and aiding physical interpretation. Yet, when evaluating many scenes at fixed spatial scales, the *L*-function distribution lacks the distinct modes expected from discrete regimes. This is corroborated by analyses of other organization indices employing diverse approaches, from inter-cloud nearest-neighbor distances to fractal analysis. Implications for the parameterization of mesoscale cloud organization in climate models are discussed.

Plain Language Summary The representation of tropical shallow cloud systems is a major source of uncertainty in climate models. Shallow clouds have previously been observed to organize in a variety of patterns. Four distinct classes—fish, flowers, sugar, and gravel—were identified, each with differing spatial scales of cloud organization. Here we analyze high-resolution geostationary visible and infrared satellite images using a function that can objectively assess organization of cloudy pixels across all spatial scales. We see that examples of the four "classical" patterns are clearly identifiable using this function, but that they do not show up as clearly preferred regimes, but rather as way-markers in a smoothly evolving sea of cloud patterns. This means that representing these patterns in parameterization schemes might be challenging.

Key Points:

- A new method based on spatial point pattern theory objectively distinguishes four established shallow cloud patterns in satellite imagery
- These patterns do not appear as modes in the distribution of cloud organization indices for a large number of scenes at fixed spatial scale
- Referring to the four patterns as distinct cloud organization regimes might constitute an oversimplification

Supporting Information:

Supporting Information may be found in the online version of this article.

Correspondence to:

G. Biagioli,
gbiagiol@ictp.it

Citation:

Biagioli, G., Mandorli, G., Freischem, L. J., Casallas, A., & Tompkins, A. M. (2026). Spatial patterns of shallow clouds: Challenging the concept of defined regimes. *Geophysical Research Letters*, *53*, e2025GL119921. https://doi.org/10.1029/2025GL119921

Received 9 OCT 2025
Accepted 25 MAR 2026

1. Introduction

Any scene of visible satellite imagery in the tropics immediately reveals a wondrous range of patterns in which clouds are organized, from small-scale shallow convective rolls and cold pools (CPs) to larger-scale systems such as hurricanes, squall-lines and planetary-scale waves. Understanding convective organization is an active area of research due to its potential impacts on climate. The spatial arrangement of clouds plays a role in shaping the atmospheric humidity distribution, the general circulation, and mean cloud cover, which in turn can modulate the Earth's radiation budget (Bony, Semie, et al., 2020). Tropical shallow clouds are particularly important, since they have a large influence on the planetary energy budget through their impact on albedo (Eastman et al., 2024; Klein & Hartmann, 1993) and are a primary cause of uncertainty in climate models (Bony & Dufresne, 2005; Myers et al., 2023; Nam et al., 2012; Vial et al., 2013).

In recent years, it has been questioned whether the mesoscale organization of shallow convection contributes to the tropical low-cloud feedback (Ceppi et al., 2017). This could represent a missing feedback mechanism, as mesoscale organization of shallow clouds is not represented in current climate model parameterizations (Mauritsen & Stevens, 2015; Schulz & Stevens, 2023). To improve our understanding and make progress toward incorporating these effects into climate models, there have been efforts to classify spatial patterns of shallow clouds.

One classification that gained significant attention identified four recurrent patterns of trade-wind cumuli in the western tropical Atlantic (Bony, Schulz, et al., 2020; Schulz et al., 2021; Stevens et al., 2020; Vogel et al., 2021),

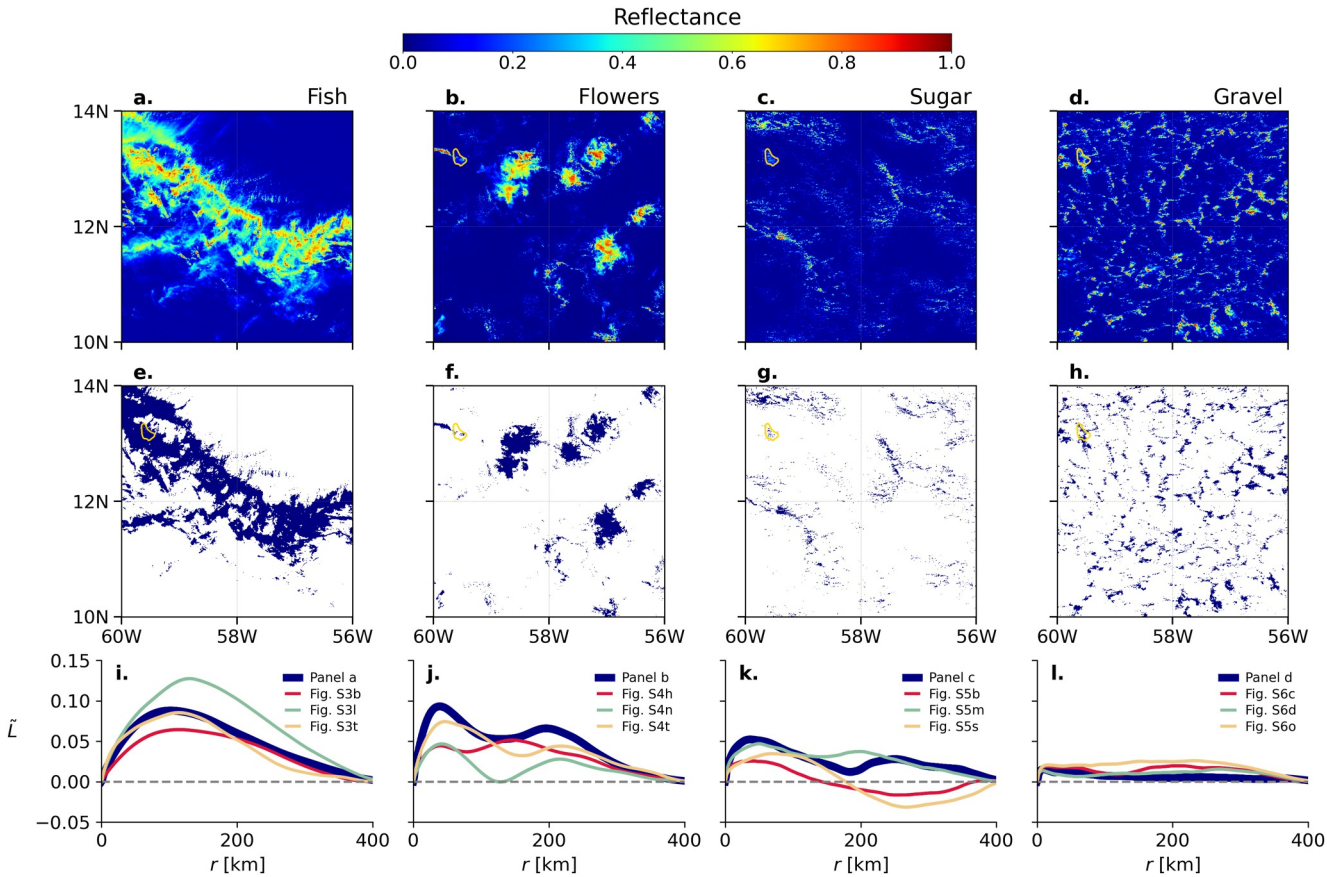

Figure 1. (a–d) 0.64 μm GOES-16 reflectance, (e–h) cloud mask, and (i–l) *L*-function for four archetypal scenes of (a, e, i) fish, (b, f, j) flowers, (c, g, k) sugar and (d, h, l) gravel, selected from the manual classification of Schulz (2022, Figures 1 and A1). In panels (a–h), the coastline is represented as a solid yellow line. In panels (i–l), the thick blue *L*-functions correspond to the scenes depicted in the same figure, while the other curves are derived from the additional scenes shown in Figures S3–S6 in Supporting Information S1, where they are identified by a color-coded horizontal bar below the panel letter. The horizontal dashed lines correspond to $\tilde{L}(r) = 0$, the *L*-function expected for random distributions of cloudy pixels.

their related evolution (Vial et al., 2021), and the mechanisms governing transitions between them (Dauhut et al., 2023; Narenpitak et al., 2021, 2023). When observed in visible satellite imagery, these patterns were named after their visual resemblance to fish, flowers, sugar, and gravel (FFSG) and characterized in terms of their spatial scales of organization (Stevens et al., 2020). We show four archetypal examples in Figures 1a–1d, using GOES geostationary visible reflectance. The "fish" pattern features long, filamentous clouds on the meso-α-scale (200−2000 km, Orlanski, 1975) resembling a fish skeleton, often with extensive stratiform regions. "Flowers" appear as quasi-regularly spaced clouds with stratiform anvils, separated by clear-sky areas. Both "sugar" and "gravel" consist of small cloud elements without anvils. According to Stevens et al. (2020), "sugar" shows "*little evidence of self-organization by cold pools or gust fronts*," whereas "gravel" is "*patterned along meso-β* (20–100 km) *lines or arcs*." However, Bony, Schulz, et al. (2020) show that "sugar" scenes are actually more clustered as measured by a cloud organization index, highlighting the subjectivity of classifications based on visual inspection and the importance of applying quantitative as well as qualitative analysis methods (Janssens et al., 2021).

The above classification was performed by manually sorting the scenes into distinct categories. This approach relied on visual inspection and subjective pattern recognition, but lacks reproducibility as it depends heavily on individual interpretation (Schulz, 2022). To overcome these issues, a supervised neural network model was developed to replicate the manual classification, allowing for rapid, consistent classification across the entire tropics (Rasp et al., 2020). However, if supervised models are trained on human labels, they inherit the subjectivity of the original classification. Additionally, classifications derived using neural networks are less directly interpretable.

A first question therefore is whether we can complement these methods using established cloud organization metrics to better quantify the differences between cloud patterns. One example is the L_{org} index (Biagioli & Tompkins, 2023), whose underlying *L*-function method assesses spatial organization across all scales in an objective and interpretable manner, identifying the dominant scales of organization. We will analyze geostationary visible and infrared satellite imagery to evaluate whether these *L*-functions can distinguish the archetypal examples of FFSG and provide a "fingerprint" for each pattern type.

The second question addressed concerns the attribution of FFSG patterns as distinct "regimes," as suggested by Stevens et al. (2020) and subsequent studies (Chatterjee et al., 2024; Fildier et al., 2023). In physics, a regime generally refers to a characteristic system behavior which is persistent relative to the time period over which transitions occur. Thus, inherent in this notion is the concept of "modes" or peaks in a probability distribution that identify the most recurrent situations (Stephenson et al., 2004).

Regimes are common in meteorology. For example, in the atmosphere the probability density function (PDF) of water droplet size is strongly multi-modal, with three well-separated regimes corresponding to sub-micron haze particles, cloud droplets (2–30 μm), and raindrops (1–3 mm) (Rogers & Yau, 1989). Strongly nonlinear processes transforming droplets rapidly between these regimes ensure it is rare to find droplets of intermediate sizes. Another example is the division of tropical convective clouds into regimes of shallow, congestus, and deep convection, corresponding to modes in the observed cloud-top height distribution (Johnson et al., 1999). This notion of regimes is more than mere semantics; the fact that regimes are distinct modes in the PDF space enables their parameterization, for instance the ability to employ bulk microphysical schemes in the former example (Lin et al., 1983), or distinct shallow and deep mass-flux convection schemes in the latter (Tiedtke, 1989).

Our second aim is therefore to determine whether the four shallow convection patterns are associated with distinct modes in the distribution of *L*-functions and common cloud organization metrics when analyzed over fixed spatial scales, and are thus classifiable as regimes. If not, cloud organization parameterizations in climate models cannot rely on discrete categories applied at their grid-scale.

The paper is organized as follows. After summarizing the *L*-function framework and other convective organization metrics (Section 2), we apply them to satellite-derived cloud fields in the region of interest and examine their scale-dependent statistical properties (Section 3.1). Next, we analyze the resulting distributions using several complementary approaches to assess whether distinct organization modes, or regimes, emerge (Sections 3.2 and 3.3). Section 4 concludes by discussing the implications for parameterizations.

2. Materials and Methods

2.1. Selection of Analysis Domains, Time Periods and Satellite Products

This study focuses on the Atlantic trade-wind region from 60°W–48°W, 8°N–18°N, divided into 20 overlapping 4° × 4° domains regularly spaced every 2°. We also assessed the sensitivity of our results to the size of the observation domains. Detailed setups for these sensitivity analyses can be found in Supporting Information S1.

During boreal winter, the region of interest is dominated by shallow convection, primarily due to the southward shift of the Intertropical Convergence Zone. Our analysis therefore used satellite observations collected during DJF seasons from December 2018 to February 2023. Reflectance data from GOES-16 channel 2 (0.64 μm) and brightness temperature (T_b) data from channel 13 (10.3 μm) were analyzed, with horizontal resolutions of 0.5 km and 2 km, respectively (Schmit et al., 2017). Despite channel 13 being available at all times of day and not affected by solar zenith angles, very fine cloud structures (e.g., sugar) might not be properly captured, as shown in Supporting Information S1, hence the preference for channel 2. To minimize the effects of sun-angle variations on reflectances, only observations at 17 UTC (13–14 local time across the study domain) were used for the analysis of channel 2 data. For consistency, observations from channel 13 were also limited to 17 UTC.

2.2. Generation of Cloud Masks

For each selected GOES scene, binary cloud masks were generated as follows. For channel 2, cloudy pixels are identified as those with a reflectance greater than 0.3. For channel 13, only those pixels with 280 K $< T_b <$ 290 K are considered cloudy. In both cases, channel 13 is further employed to exclude scenes with excessive high

cloudiness by rejecting images where the 10th percentile of T_b is below 280 K. This combined selection process ensures the generation of image masks specifically representing shallow clouds and is consistent with the criteria adopted in previous studies (Bony, Schulz, et al., 2020; Schulz, 2022). In terms of sample sizes, of the initial 8960 GOES-16 channel 2 images considered, 1993 were excluded due to excessive high cloud contamination, leaving a total of 6967 images. This data set comprises both FFSG examples and unclassified scenes.

2.3. Selection of Archetypal Scenes

To analyze FFSG patterns, we selected 20 archetypal scenes per class from the manual classification of Schulz (2022, Figure A1), including the four representative examples shown in Figure 1. Selection criteria included clear pattern dominance within the $4° \times 4°$ domains and moderate-to-high inter-classifier agreement. Scenes are geographically non-overlapping to ensure statistical independence. The full set of archetypal scenes is displayed in Figures S3–S6 in Supporting Information S1.

2.4. The *L*-Function

The present analysis makes use of the Besag's *L*-function (Besag, 1977), a tool from point pattern theory that summarizes the spatial distribution of a two-dimensional pattern across scales. The *L*-function quantifies the average number of neighbors within distance r of any point of the pattern relative to the expectation for a random distribution. More (fewer) neighbors than expected indicate clustering (regularity) of the pattern at scale r. In our study, the points correspond to cloud pixel centroids. The *L*-function's multi-scale nature makes it particularly suited for analyzing cloud patterns whose organization varies across scales. For example, for flowers, characterized by clusters of clouds separated by large clear-sky areas, the *L*-function is expected to indicate clustering at the scale of individual aggregates and a tendency toward regularity at the scale of inter-cluster gaps. In contrast, the elongated cloud structures of fish are expected to be reflected in the *L*-function as a clustering signal at all scales.

The *L*-functions are computed directly from the binary cloud masks defined above, with no connectivity-clustering applied, so that adjacent cloudy pixels are treated individually. This choice reflects the small size of shallow cloud elements, often near sensor resolution, where merging could artificially combine distinct elements, distorting spatial statistics.

This study uses the framework of Biagioli and Tompkins (2023), analyzing *L*-functions over fixed domains with various geometries and accounting for boundary conditions. For gridded satellite data, neighbors of each cloudy pixel are counted within square observation boxes of increasing apothem r, with counts corrected for edge effects to avoid underestimations near domain boundaries. The procedure is repeated for each base pixel, and at each scale r the neighbor counts are averaged across all base elements. The resulting averaged counts are then normalized by the overall cloud spatial density. The *L*-function $\tilde{L}(r)$ is finally obtained from this scale-dependent measure by taking the square root and subtracting the expected value at each scale under a random distribution of the same number of cloud elements. Values of $\tilde{L}(r) > 0$ ($\tilde{L}(r) < 0$) indicate clustering (regularity) at scale r, while $\tilde{L}(r) = 0$ represents randomness. The mathematical details of *L*-function computation are provided in Supporting Information S1.

Previous studies used visual typing, machine learning, and more quantitative approaches such as convective organization metrics or nearest-neighbor cumulative distribution functions (NNCDFs) to analyze shallow cloud patterns. Unlike single-value metrics and the NNCDF, which emphasizes the very short-range behavior of the cloud field and may fail to discriminate visually distinct patterns (e.g., Figure S1 of Bony, Schulz, et al., 2020), the *L*-function encapsulates the multi-scale spatial organization of clouds within a single unified framework. This is particularly advantageous given that previous studies suggest convective organization may require multiple dimensions to be fully characterized (e.g., Brune et al., 2018; Janssens et al., 2021; Pscheidt et al., 2019). Another key strength of the present method is the existence of a theoretical null hypothesis against which to evaluate the observed scene. In conclusion, the *L*-function provides a concise, objective, and interpretable summary of cloud patterns across all spatial scales.

Table 1
Cloud Organization Indices Used in This Study

Index	Overview	Input	References
L_{org}	Integral of $\tilde{L}(r)$, normalized by the domain size. It provides an integrated assessment of organization across all spatial scales up to the domain size, values larger than 0 indicate clustering.	Cloud mask pixels	Biagioli and Tompkins (2023)
SCAI	Simple Convective Aggregation Index, proportional to the number of cloud clusters and their grouping as measured by the geometric mean distance between cluster centroids.	Cloud mask objects	Tobin et al. (2012, 2013)
COP	Convective Organization Potential, analogous to the gravitational potential, calculated using equivalent radii of cloud objects and their inter-centroid distances.	Cloud mask objects	White et al. (2018)
ABCOP	Area-based COP, a variant of COP that assigns different weights to the number and area of cloud objects. It uses edge-to-edge separation distances rather than centroid distances.	Cloud mask objects	Jin et al. (2022)
ROME	Radar Organization Metric, a variant of COP that is a linear combination of cloud cluster areas, weighted by a factor accounting for the areas in-between that serve as a measure of object proximity.	Cloud mask objects	Retsch et al. (2020)
I_{org}	Index based on the comparison of the cumulative distribution function (CDF) of cloud-cloud nearest-neighbor distances in a scene to the reference of a spatial Poisson point process. I_{org} is the integral of the joint CDF, values larger than 0.5 indicate clustered states.	Cloud mask objects	Seifert and Heus (2013), Tompkins and Semie (2017)
OIDRA	Organization Index based on Distance and Relative Area, that considers cloud object relative areas and distances, with greater emphasis placed on larger distances than smaller ones.	Cloud mask objects	Mandorli and Stubenrauch (2024)
ζ_∞	Multifractal scaling parameter, that quantifies convective organization using spatial variability of radiances within an image. Values larger than 1 indicate clustered cloud fields, while lower values indicate disorganized convection. The fitting range used to derive the parameter is 4–16 km (see reference).	Direct radiances	Freischem et al. (2024), Pierrehumbert (1996)

2.5. Convective Organization Metrics

The level of convective organization observed from a satellite scene can be determined through scalar-valued metrics, or indices, that measure the spatial distribution of cloud entities in a quantitative way, distinguishing clustered from scattered patterns. Some indices are computed directly from horizontal fields of meteorological variables, others are derived from two-dimensional pixel-level binary cloud masks, and others require applying connectivity-clustering algorithms to merge adjacent convective pixels into distinct cloud objects.

In the present analysis, we considered the pixel-based L_{org} index derived from L-functions, several object-based indices, and an index assessing the fractal statistics of spatial variability directly from observed radiances, which avoids any thresholding to define cloudy pixels. Table 1 provides a brief description of the indices used and their references (see also Biagioli & Tompkins, 2023; Mandorli & Stubenrauch, 2024). All indices were computed following the original definitions and procedures, without significant modifications. All described metrics, except for SCAI, indicate more clustered conditions with higher values. Apart from I_{org} and L_{org}, all indices are relative; that is, they cannot assess clustering relative to a null hypothesis of randomness.

3. Results

3.1. Fish, Flowers, Sugar, and Gravel in the L-Function Space

We analyze satellite images representing the established patterns of FFSG, considering a subset of four representative examples per class selected from the 20 archetypal scenes defined in Section 2.3. Figure 1 shows observed reflectance and corresponding cloud masks for one example per category, with the additional cases illustrated in Figures S3–S6 in Supporting Information S1. For each scene, we derive the L-function from the binary cloud mask.

The L-function exhibits distinct characteristics for each of the four patterns. For fish (panel i), it shows strong clustering at all spatial scales. The function is smooth and unimodal, with the peak representing the scale of maximum clustering occurring at $\mathcal{O}$(100–150 km), indicative of the cross-sectional scale of the fish pattern. The peak thus gives us an immediate measure of the fish scale.

All L-functions associated with flowers are instead multi-modal (Figure 1j). The first peak appears at small scales (~50 km), corresponding to the typical flower anvil cloud radius. The second peak reflects the average inter-centroid distance between flower aggregates, which, although not strictly identical across scenes, falls within a relatively narrow range. Its prominence varies across scenes, due to differences in the size and spacing of flower elements. The relative minimum of $\tilde{L}(r)$, occurring at scales of 80–150 km with scene-to-scene variability, corresponds to clear-sky areas surrounding individual flowers. It is more pronounced in scenes where the flowers are more widely separated. The distance between local extrema is therefore indicative of the scale of the shallow circulation that develops at cloud scale, $\mathcal{O}$(100 km), consistent with George et al. (2023). As shown in Supporting Information S1, temporal analysis demonstrates that the bimodality strengthens as individual flowers grow and the spacing in-between becomes more consistent, hinting at the roles of convective inhibition by large-scale CPs and the emergence of long-lived mesoscale circulations that amplify the spatial heterogeneities in the vapor field, reducing shallow cloud occurrence around flowers (Figure S9 in Supporting Information S1). This interpretation aligns with previous observational and modeling studies (Bony et al., 2025; Dauhut et al., 2023; Narenpitak et al., 2021; Touzé-Peiffer et al., 2022).

The sugar category exhibits the largest variability in L-functions (panel k). These functions have either a single peak or multiple peaks but are not as smooth as for flowers. They may span a wide range of organization levels, including both high and low degrees, sometimes even showing regularity at certain scales. Despite this variability, the overall degree of organization in sugar patterns tends to be higher than in gravel, but lower than in fish and flowers.

Lastly, the L-functions associated with gravel (Figure 1l) are generally flat, indicating low levels of organization across scales. They typically show a minor peak at 20–30 km, observed in the majority of selected archetypal scenes, corresponding to the size of the intermediate-granularity objects seen in Figures 1d and 1h. This scale-specific clustering signal could arise from local processes such as turbulent updraft interactions or CPs (Stevens et al., 2020). Subsequent slight decreases in L-functions reflect the reduction in shallow clouds in the vicinity of gravel elements, which Bony et al. (2025) attributed to relatively strong circulations that develop at cloud scale. At larger scales, a tendency toward nearly random organization is observed, as cloud elements are uniformly distributed within the domain. Among the four patterns, the L-functions for gravel exhibit the least variability, indicating a more uniform behavior within this category.

In summary, the L-functions display distinct characteristics for each category, emphasizing the unique horizontal convection patterns of FFSG. These examples also show that, although inherently geometrical, the L-function captures scale-dependent fingerprints of the underlying physical processes and, when interpreted together with environmental variables, can offer insight into the mechanisms controlling cloud organization.

3.2. Are Fish, Flowers, Sugar, and Gravel Cloud Organization Regimes?

Can the four archetypal categories be referred to as regimes, that is, are the distinct L-function shapes manifested as well-defined modes in L-function distribution space? To address this question, we computed ensemble-mean L-functions for each class using the 20 archetypal scenes per class defined in Section 2.3, along with their variability (mean ± standard deviation; Figures 2a–2d). While the ensemble-mean L-functions generally differ between classes, the variability ranges overlap across multiple spatial scales. Therefore, although FFSG patterns provide a useful qualitative description of cloud morphology, they do not correspond to distinct classes in L-function space.

For each fixed scale r, we then compute the PDF of $\tilde{L}(r)$ values across all available scenes spanning five DJF seasons (Figure 2e). The PDF represents the scene-to-scene variability of $\tilde{L}(r)$ at scale r and includes all archetypal examples. The highest degrees of clustering at scales of 100–150 km are likely contributed to by fish-like patterns, while the tendency to observe cloud field regularity at scales exceeding 200 km in some scenes might indicate the presence of sugar. The highest densities at 20–100 km are found for $\tilde{L}(r) \approx 0.05$, possibly indicating a predominance of sugar at those scales in the collection of scenes. This is consistent with the previous manual classification (Stevens et al., 2020), which reported sugar in every image, though often confined to small patches of $\mathcal{O}$(10 km) in horizontal extent. For this reason, we tested the sensitivity of our results to different sizes of the observation windows and different resolutions, but no significant variations were found, as shown in Supporting Information S1.

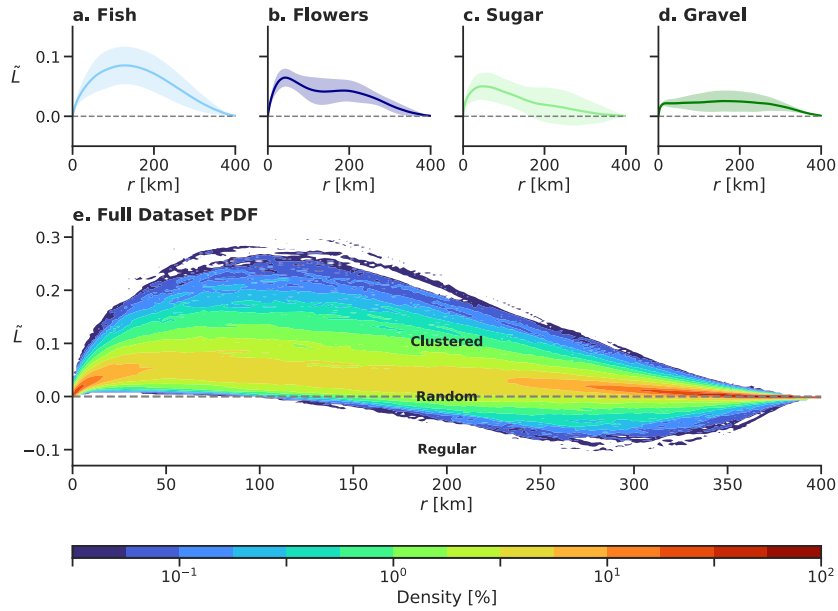

Figure 2. (a–d) Ensemble-mean *L*-functions for the four fish, flowers, sugar, and gravel classes, computed from the 20 archetypal scenes per class defined in Section 2.3. Shading indicates mean ± one standard deviation. (e) Probability density function of *L*-function values at each fixed spatial scale *r*, computed from all GOES-16 visible scenes spanning DJF seasons in the period December 2018-February 2023.

Overall, Figure 2e reveals that the four patterns of mesoscale shallow convective organization do not emerge as modes in the *L*-function distribution, as no evidence is found for multiple groups of scenes with similar-looking *L*-functions occurring more frequently than others. This demonstrates that the organization space is unimodal overall. Thus, although the visual inspection of the functions can provide useful information on the spatial tendencies of a given scene, it seems questionable that the four classes constitute regimes. This result is further supported by additional analysis we conducted on all available *L*-functions including a principal component analysis and the application of hierarchical clustering algorithms, an effective method for identifying potential clusters or assessing data unimodality by iteratively grouping data points based on similarity, with the results detailed in Supporting Information S1.

Our findings are consistent with previous studies, such as Bony, Schulz, et al. (2020), where scenes appeared continuous in I_{org} space, and Janssens et al. (2021) who claimed that breaking the continuum of cloud organization into four classes is rather arbitrary. Unimodality also aligns with recent findings from unsupervised (Denby, 2020) and self-supervised (Chatterjee et al., 2024) neural network models, which reveal a continuous distribution of scenes throughout the output space.

3.3. Robustness Across a Range of Alternative Organization Indices

We generalize the analysis to encompass a wide range of commonly used organization indices (Biagioli & Tompkins, 2023; Mandorli & Stubenrauch, 2024), eight of which are shown in Figure 3. For all indices, the distributions are unimodal and, as with $\tilde{L}(r)$, there are no signs of separate modes corresponding to the four organization classes. This holds irrespective of the domain size, satellite channel analyzed, and also for a different set of organization metrics, as documented in Supporting Information S1. We also examined selected two-dimensional combinations of indices, but these likewise fail to reveal distinct modes (Figure S18 in Supporting Information S1).

The distributions of the indices are quite disparate, in that some are symmetrical (e.g., I_{org}), while the others are skewed. On each panel, the colored marks represent the 16 archetypal scenes analyzed in Figure 1. For most indices, the values for these 16 scenes span most of the distribution function space. In some cases, there are indications that the metric can differentiate between the four classes, that is, scenes corresponding to the four

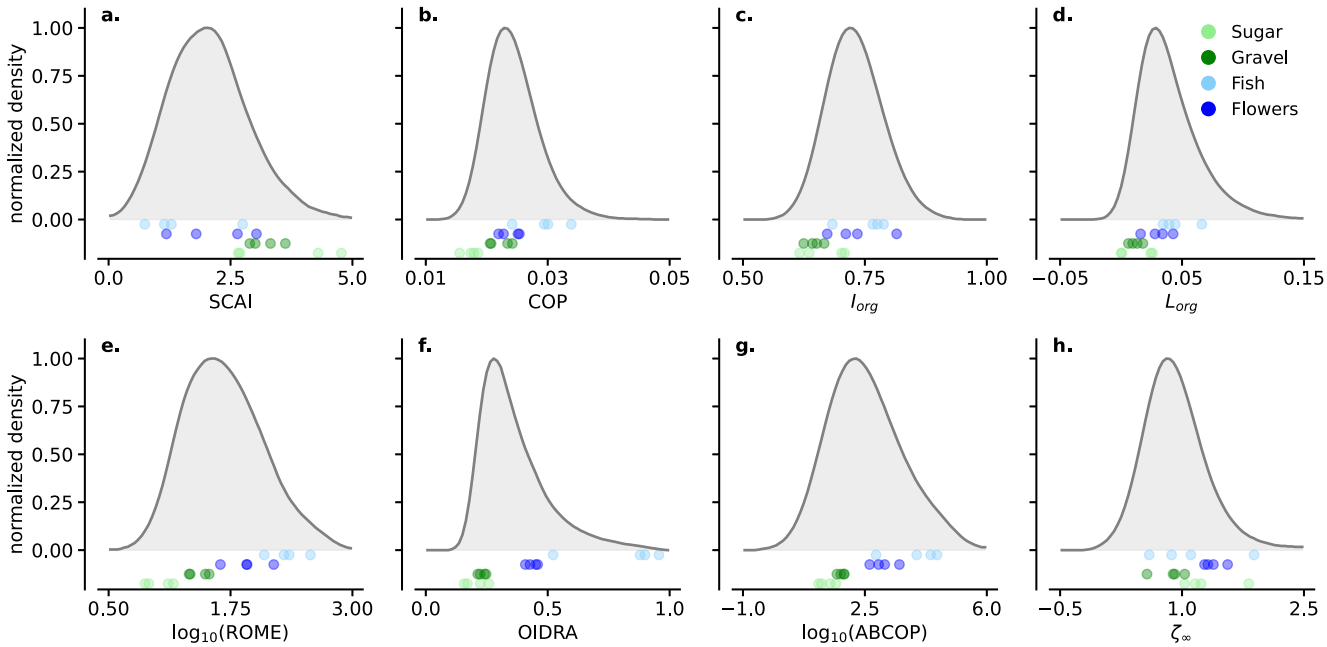

Figure 3. Distribution of the organization metrics (a) SCAI, (b) COP, (c) I_{org}, (d)L_{org}, (e) $\log_{10}$(ROME), (f) OIDRA, (g) $\log_{10}$(ABCOP), and (h) ζ_∞. The *y*-axis represents the relative frequency of occurrences, and it is normalized to a maximum value of 1. The colored marks show the values corresponding to the 16 representative scenes of the four organization classes considered in Figure 1.

classes tend to occupy distinct regions of the metric space. However, overlaps between classes are observed across all metrics.

4. Discussion and Conclusions

Previous work attempted to sort individual satellite scenes of trade-wind shallow cloudiness into four distinct classes of spatial organization. By doing so, one might attempt to understand the organization in terms of specific dynamic/thermodynamic processes and simplify the problem of cloud arrangement to make it tractable for parameterization purposes and inclusion into climate models. Such an end-goal is likely important if changes to cloud arrangements occur in a warming climate, which can act as a missing feedback.

We have examined these four classes in terms of a recently derived analysis method based on the statistical theory of spatial point patterns (Illian et al., 2008; Stoyan et al., 2013). The method employs a function, the *L*-function, computed from the point-to-point distances of all cloudy pixels in a scene (Besag, 1977; Biagioli & Tompkins, 2023). It provides an objective, physically interpretable, scale-dependent characterization of spatial cloud organization, without the need to invoke arbitrary rules for point connectivity, and enables direct comparison to a null-hypothesis model of random organization.

The *L*-function analysis has proven useful; satellite scenes clearly identifiable by visual inspection as archetypal examples of the four FFSG patterns could be neatly distinguished from each other with the specific fingerprint of their associated *L*-function. This approach also captures the dominant spatial scales of organization for each pattern and their evolution. However, when examining the aggregate distribution of *L*-functions for a large collection of scenes of specific spatial dimension, there was no sign of distinct modes required to define physical regimes. Similarly, no modes emerged from the PDFs of a wide variety of organization indices. This latter finding is independent of the *L*-function analysis and confirms the ubiquitous presence of unimodality in cloud organization statistics when analyzed over fixed mesoscale domains relevant for climate models.

The absence of distinct regimes has fundamental implications for the philosophy of parameterization design. It challenges the feasibility of "trigger-based" approaches, where a model attempts to detect a specific regime and switch to a corresponding physical scheme. Because the transitions between patterns are smooth and continuous, imposing artificial thresholds would likely introduce spurious bifurcations and instability in model behavior.

Instead, our findings suggest that parameterization efforts should shift away from discrete classification toward representing sub-grid heterogeneity as a continuous distribution or dynamic mixture. Practically, this supports a time-varying "tiled" approach—similar to those used in land-surface modeling (Krinner et al., 2005), where a grid box comprises fractional coverages of different patterns rather than a single dominant type. In fact, since the four classes have inherently different horizontal scales, as found by Stevens et al. (2020) and quantitatively confirmed by our *L*-function analysis, the observed unimodality of organization may result from the combination of discrete categories in variable proportions. By predicting the weighting of these tiles (or the moments of the sub-grid probability distribution) rather than toggling between binary regimes, models can faithfully represent the continuum of organization observed in nature. Recent success in modeling these shallow cloud systems with high-resolution large-eddy simulations (Dauhut et al., 2023) suggests that progress in this direction is achievable.

Conflict of Interest

The authors declare no conflicts of interest relevant to this study.

Availability Statement

GOES-16 data are available at https://noaa-goes16.s3.amazonaws.com/index.html. The code used for computing *L*-functions is available from Biagioli (2026), for other organization metrics and the multifractal scaling parameter, the reader can refer to the data availability statements of Mandorli and Stubenrauch (2024) and Freischem et al. (2024), respectively.

Acknowledgments
GB was supported by an ICTP Postdoctoral Research Fellowship Agreement. GM was supported by the CNRS. AC was supported by the European Union's Horizon 2020 research and innovation programme Marie Sklodowska-Curie Grant agreement No 101034413. LJF acknowledges funding from the NERC Doctoral Training Partnership in Environmental Research Grant NE/S007474/1. We thank three anonymous reviewers and Jiawei Bao for their insightful comments, which greatly improved this manuscript.

References

Besag, J. (1977). Contribution to the discussion on Dr. Ripley's paper. *Journal of the Royal Statistical Society: Series B*, *39*(2), 193–195. https://doi.org/10.1111/j.2517-6161.1977.tb01616.x

Biagioli, G. (2026). giobiagioli/organization_indices: Version 2.0.0: Major code update (v2.0.0) [Software]. *Zenodo*. https://doi.org/10.5281/zenodo.18319310

Biagioli, G., & Tompkins, A. M. (2023). Measuring convective organization. *Journal of the Atmospheric Sciences*, *80*(12), 2769–2789. https://doi.org/10.1175/JAS-D-23-0103.1

Bony, S., & Dufresne, J.-L. (2005). Marine boundary layer clouds at the heart of tropical cloud feedback uncertainties in climate models. *Geophysical Research Letters*, *32*(20). https://doi.org/10.1029/2005gl023851

Bony, S., Poujol, B., McKim, B., Rochetin, N., Lothon, M., Windmiller, J., et al. (2025). Evidence for the role of thermal and cloud merging in mesoscale convective organization. *Atmospheric Chemistry and Physics*, *25*(23), 17331–17362. https://doi.org/10.5194/acp-25-17331-2025

Bony, S., Schulz, H., Vial, J., & Stevens, B. (2020). Sugar, gravel, fish, and flowers: Dependence of mesoscale patterns of trade-wind clouds on environmental conditions. *Geophysical Research Letters*, *47*(7), e2019GL085988. https://doi.org/10.1029/2019GL085988

Bony, S., Semie, A., Kramer, R. J., Soden, B., Tompkins, A. M., & Emanuel, K. A. (2020). Observed modulation of the tropical radiation budget by deep convective organization and lower-tropospheric stability. *AGU Advances*, *1*(3), e2019AV000155. https://doi.org/10.1029/2019AV000155

Brune, S., Kapp, F., & Friederichs, P. (2018). A wavelet-based analysis of convective organization in ICON large-eddy simulations. *Quarterly Journal of the Royal Meteorological Society*, *144*(717), 2812–2829. https://doi.org/10.1002/qj.3409

Ceppi, P., Brient, F., Zelinka, M. D., & Hartmann, D. L. (2017). Cloud feedback mechanisms and their representation in global climate models. *WIREs Climate Change*, *8*(4), e465. https://doi.org/10.1002/wcc.465

Chatterjee, D., Schnitt, S., Bigalke, P., Acquistapace, C., & Crewell, S. (2024). Capturing the diversity of mesoscale trade wind cumuli using complementary approaches from self-supervised deep learning. *Geophysical Research Letters*, *51*(12), e2024GL108889. https://doi.org/10.1029/2024GL108889

Dauhut, T., Couvreux, F., Bouniol, D., Beucher, F., Volkmer, L., Pörtge, V., et al. (2023). Flower trade-wind clouds are shallow mesoscale convective systems. *Quarterly Journal of the Royal Meteorological Society*, *149*(750), 325–347. https://doi.org/10.1002/qj.4409

Denby, L. (2020). Discovering the importance of mesoscale cloud organization through unsupervised classification. *Geophysical Research Letters*, *47*(1), e2019GL085190. https://doi.org/10.1029/2019GL085190

Eastman, R., McCoy, I. L., Schulz, H., & Wood, R. (2024). A survey of radiative and physical properties of North Atlantic mesoscale cloud morphologies from multiple identification methodologies. *Atmospheric Chemistry and Physics*, *24*(11), 6613–6634. https://doi.org/10.5194/acp-24-6613-2024

Fildier, B., Muller, C., Pincus, R., & Fueglistaler, S. (2023). How moisture shapes low-level radiative cooling in subsidence regimes. *AGU Advances*, *4*(3), e2023AV000880. https://doi.org/10.1029/2023AV000880

Freischem, L. J., Weiss, P., Christensen, H. M., & Stier, P. (2024). Multifractal analysis for evaluating the representation of clouds in global kilometer-scale models. *Geophysical Research Letters*, *51*(20), e2024GL110124. https://doi.org/10.1029/2024GL110124

George, G., Stevens, B., Bony, S., Vogel, R., & Naumann, A. K. (2023). Widespread shallow mesoscale circulations observed in the trades. *Nature Geoscience*, *16*(7), 584–589. https://doi.org/10.1038/s41561-023-01215-1

Illian, J., Penttinen, A., Stoyan, H., & Stoyan, D. (2008). *Statistical analysis and modelling of spatial point patterns*. Wiley. https://doi.org/10.1002/9780470725160

Janssens, M., Vilà-Guerau de Arellano, J., Scheffer, M., Antonissen, C., Siebesma, A. P., & Glassmeier, F. (2021). Cloud patterns in the trades have four interpretable dimensions. *Geophysical Research Letters*, *48*(5), e2020GL091001. https://doi.org/10.1029/2020GL091001

Jin, D., Oreopoulos, L., Lee, D., Tan, J., & Kim, K.-M. (2022). A new organization metric for synoptic scale tropical convective aggregation. *Journal of Geophysical Research: Atmospheres*, *127*(13), e2022JD036665. https://doi.org/10.1029/2022JD036665

Johnson, R. H., Rickenbach, T. M., Rutledge, S. A., Ciesielski, P. E., & Schubert, W. H. (1999). Trimodal characteristics of tropical convection. *Journal of Climate*, *12*(8), 2397–2418. https://doi.org/10.1175/1520-0442(1999)012⟨2397:TCOTC⟩2.0.CO;2

Klein, S. A., & Hartmann, D. L. (1993). The seasonal cycle of low stratiform clouds. *Journal of Climate*, *6*(8), 1587–1606. https://doi.org/10.1175/1520-0442(1993)006⟨1587:TSCOLS⟩2.0.CO;2

Krinner, G., Viovy, N., de Noblet-Ducoudré, N., Ogée, J., Polcher, J., Friedlingstein, P., & Prentice, I. C. (2005). A dynamic global vegetation model for studies of the coupled atmosphere-biosphere system. *Global Biogeochemical Cycles*, *19*(1). https://doi.org/10.1029/2003GB002199

Lin, Y.-L., Farley, R. D., & Orville, H. D. (1983). Bulk parameterization of the snow field in a cloud model. *Journal of Climate and Applied Meteorology*, *22*(6), 1065–1092. https://doi.org/10.1175/1520-0450(1983)022⟨1065:BPOTSF⟩2.0.CO;2

Mandorli, G., & Stubenrauch, C. J. (2024). Assessment of object-based indices to identify convective organization. *Geoscientific Model Development*, *17*(21), 7795–7813. https://doi.org/10.5194/gmd-17-7795-2024

Mauritsen, T., & Stevens, B. (2015). Missing Iris effect as a possible cause of muted hydrological change and high climate sensitivity in models. *Nature Geoscience*, *8*(5), 346–351. https://doi.org/10.1038/ngeo2414

Myers, T. A., Zelinka, M. D., & Klein, S. A. (2023). Observational constraints on the cloud feedback pattern effect. *Journal of Climate*, *36*(18), 6533–6545. https://doi.org/10.1175/JCLI-D-22-0862.1

Nam, C., Bony, S., Dufresne, J.-L., & Chepfer, H. (2012). The too few, too bright tropical low-cloud problem in CMIP5 models. *Geophysical Research Letters*, *39*(21). https://doi.org/10.1029/2012GL053421

Narenpitak, P., Kazil, J., Yamaguchi, T., Quinn, P., & Feingold, G. (2021). From sugar to flowers: A transition of shallow cumulus organization during ATOMIC. *Journal of Advances in Modeling Earth Systems*, *13*(10), e2021MS002619. https://doi.org/10.1029/2021ms002619

Narenpitak, P., Kazil, J., Yamaguchi, T., Quinn, P. K., & Feingold, G. (2023). The sugar-to-flower shallow cumulus transition under the influences of diel cycle and free-tropospheric mineral dust. *Journal of Advances in Modeling Earth Systems*, *15*(1), e2022MS003228. https://doi.org/10.1029/2022MS003228

Orlanski, I. (1975). A rational subdivision of scales for atmospheric processes. *Bulletin of the American Meteorological Society*, *56*(5), 527–530. https://doi.org/10.1175/1520-0477-56.5.527

Pierrehumbert, R. T. (1996). Anomalous scaling of high cloud variability in the tropical Pacific. *Geophysical Research Letters*, *23*(10), 1095–1098. https://doi.org/10.1029/96GL01121

Pscheidt, I., Senf, F., Heinze, R., Deneke, H., Trömel, S., & Hohenegger, C. (2019). How organized is deep convection over Germany? *Quarterly Journal of the Royal Meteorological Society*, *145*(723), 2366–2384. https://doi.org/10.1002/qj.3552

Rasp, S., Schulz, H., Bony, S., & Stevens, B. (2020). Combining crowdsourcing and deep learning to explore the mesoscale organization of shallow convection. *Bulletin of the American Meteorological Society*, *101*(11), E1980–E1995. https://doi.org/10.1175/BAMS-D-19-0324.1

Retsch, M. H., Jakob, C., & Singh, M. (2020). Assessing convective organization in tropical radar observations. *Journal of Geophysical Research: Atmospheres*, *125*(7), e2019JD031801. https://doi.org/10.1029/2019JD031801

Rogers, R. R., & Yau, M. K. (1989). *A short course in cloud physics*. Butterworth-Heinemann.

Schmit, T. J., Griffith, P., Gunshor, M. M., Daniels, J. M., Goodman, S. J., & Lebair, W. J. (2017). A closer look at the ABI on the GOES-R series. *Bulletin of the American Meteorological Society*, *98*(4), 681–698. https://doi.org/10.1175/BAMS-D-15-00230.1

Schulz, H. (2022). C^{3}ONTEXT: A common consensus on convective OrgaNizaTion during the EUREC^{4}A eXperimenT. *Earth System Science Data*, *14*(3), 1233–1256. https://doi.org/10.5194/essd-14-1233-2022

Schulz, H., Eastman, R., & Stevens, B. (2021). Characterization and evolution of organized shallow convection in the downstream north Atlantic trades. *Journal of Geophysical Research: Atmospheres*, *126*(17), e2021JD034575. https://doi.org/10.1029/2021JD034575

Schulz, H., & Stevens, B. (2023). Evaluating large-domain, hecto-meter, large-eddy simulations of trade-wind clouds using EUREC^{4}A data. *Journal of Advances in Modeling Earth Systems*, *15*(10), e2023MS003648. https://doi.org/10.1029/2023MS003648

Seifert, A., & Heus, T. (2013). Large-eddy simulation of organized precipitating trade wind cumulus clouds. *Atmospheric Chemistry and Physics*, *13*(11), 5631–5645. https://doi.org/10.5194/acp-13-5631-2013

Stephenson, D. B., Hannachi, A., & O'Neill, A. (2004). On the existence of multiple climate regimes. *Quarterly Journal of the Royal Meteorological Society*, *130*(597), 583–605. https://doi.org/10.1256/qj.02.146

Stevens, B., Bony, S., Brogniez, H., Hentgen, L., Hohenegger, C., Kiemle, C., et al. (2020). Sugar, gravel, fish and flowers: Mesoscale cloud patterns in the trade winds. *Quarterly Journal of the Royal Meteorological Society*, *146*(726), 141–152. https://doi.org/10.1002/qj.3662

Stoyan, D., Kendall, W., Chiu, S., & Mecke, J. (2013). *Stochastic geometry and its applications* (3rd ed.). Wiley. https://doi.org/10.1002/9781118658222

Tiedtke, M. (1989). A comprehensive mass flux scheme for cumulus parameterization in large-scale models. *Monthly Weather Review*, *117*(8), 1779–1800. https://doi.org/10.1175/1520-0493(1989)117<1779:acmfsf>2.0.co;2

Tobin, I., Bony, S., Holloway, C. E., Grandpeix, J.-Y., Sèze, G., Coppin, D., et al. (2013). Does convective aggregation need to be represented in cumulus parameterizations? *Journal of Advances in Modeling Earth Systems*, *5*(4), 692–703. https://doi.org/10.1002/jame.20047

Tobin, I., Bony, S., & Roca, R. (2012). Observational evidence for relationships between the degree of aggregation of deep convection, water vapor, surface fluxes, and radiation. *Journal of Climate*, *25*(20), 6885–6904. https://doi.org/10.1175/JCLI-D-11-00258.1

Tompkins, A. M., & Semie, A. G. (2017). Organization of tropical convection in low vertical wind shears: Role of updraft entrainment. *Journal of Advances in Modeling Earth Systems*, *9*(2), 1046–1068. https://doi.org/10.1002/2016MS000802

Touzé-Peiffer, L., Vogel, R., & Rochetin, N. (2022). Cold pools observed during EUREC^{4}A: Detection and characterization from atmospheric soundings. *Journal of Applied Meteorology and Climatology*, *61*(5), 593–610. https://doi.org/10.1175/JAMC-D-21-0048.1

Vial, J., Dufresne, J.-L., & Bony, S. (2013). On the interpretation of inter-model spread in CMIP5 climate sensitivity estimates. *Climate Dynamics*, *41*(11), 3339–3362. https://doi.org/10.1007/s00382-013-1725-9

Vial, J., Vogel, R., & Schulz, H. (2021). On the daily cycle of mesoscale cloud organization in the winter trades. *Quarterly Journal of the Royal Meteorological Society*, *147*(738), 2850–2873. https://doi.org/10.1002/qj.4103

Vogel, R., Konow, H., Schulz, H., & Zuidema, P. (2021). A climatology of trade-wind cumulus cold pools and their link to mesoscale cloud organization. *Atmospheric Chemistry and Physics*, *21*(21), 16609–16630. https://doi.org/10.5194/acp-21-16609-2021

White, B. A., Buchanan, A. M., Birch, C. E., Stier, P., & Pearson, K. J. (2018). Quantifying the effects of horizontal grid length and parameterized convection on the degree of convective organization using a metric of the potential for convective interaction. *Journal of the Atmospheric Sciences*, *75*(2), 425–450. https://doi.org/10.1175/JAS-D-16-0307.1

References From the Supporting Information

Aloise, D., Deshpande, A., Hansen, P., & Popat, P. (2009). NP-hardness of Euclidean sum-of-squares clustering. *Machine Learning*, *75*(2), 245–248. https://doi.org/10.1007/s10994-009-5103-0

Chan, S. C., Kendon, E. J., Fowler, H. J., Blenkinsop, S., Ferro, C. A. T., & Stephenson, D. B. (2013). Does increasing the spatial resolution of a regional climate model improve the simulated daily precipitation? *Climate Dynamics*, *41*(5), 1475–1495. https://doi.org/10.1007/s00382-012-1568-9

Cohen, B. G., & Craig, G. C. (2006). Fluctuations in an equilibrium convective ensemble. Part II: Numerical experiments. *Journal of the Atmospheric Sciences*, *63*(8), 2005–2015. https://doi.org/10.1175/JAS3710.1

Davies, D. L., & Bouldin, D. W. (1979). A cluster separation measure. *IEEE Transactions on Pattern Analysis and Machine Intelligence*, *PAMI-1*(2), 224–227. https://doi.org/10.1109/TPAMI.1979.4766909

Kadoya, T., & Masunaga, H. (2018). New observational metrics of convective self-aggregation: Methodology and a case study. *Journal of the Meteorological Society of Japan. Series II*, *96*(6), 535–548. https://doi.org/10.2151/jmsj.2018-054

Nair, U. S., Weger, R. C., Kuo, K. S., & Welch, R. M. (1998). Clustering, randomness, and regularity in cloud fields: 5. The nature of regular cumulus cloud fields. *Journal of Geophysical Research*, *103*(D10), 11363–11380. https://doi.org/10.1029/98JD00088

Steinbach, M., Karypis, G., & Kumar, V. (2000). *A comparison of document clustering techniques (tech. Rep. No. TR 00-034)*. University of Minnesota. Retrieved from https://conservancy.umn.edu/items/76f0aaa8-bbf7-4c9f-bec2-3ce7a3227c9d

Weger, R. C., Lee, J., Zhu, T., & Welch, R. M. (1992). Clustering, randomness and regularity in cloud fields: 1. Theoretical considerations. *Journal of Geophysical Research*, *97*(D18), 20519–20536. https://doi.org/10.1029/92jd02038

Xu, K.-M., Hu, Y., & Wong, T. (2019). Convective aggregation and indices examined from CERES cloud object data. *Journal of Geophysical Research: Atmospheres*, *124*(24), 13604–13624. https://doi.org/10.1029/2019JD030816